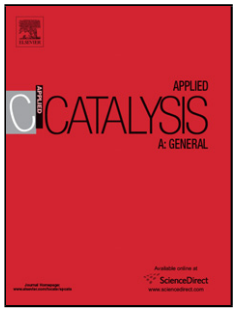

Title: Insight into the role of hydroxyl groups on the ZnCr catalyst for isobutanol synthesis from syngas

Authors: Xiaofeng Gao, Yingquan Wu, Guohui Yang, Tao Zhang, Xiaoli Li, Hongjuan Xie, Junxuan Pan, Yisheng Tan

PII: S0926-860X(17)30402-7
DOI: http://dx.doi.org/10.1016/j.apcata.2017.08.022
Reference: APCATA 16377

To appear in: *Applied Catalysis A: General*

Received date: 31-5-2017
Revised date: 11-8-2017
Accepted date: 15-8-2017

Please cite this article as: Xiaofeng Gao, Yingquan Wu, Guohui Yang, Tao Zhang, Xiaoli Li, Hongjuan Xie, Junxuan Pan, Yisheng Tan, Insight into the role of hydroxyl groups on the ZnCr catalyst for isobutanol synthesis from syngas, Applied Catalysis A, Generalhttp://dx.doi.org/10.1016/j.apcata.2017.08.022

Insight into the role of hydroxyl groups on the ZnCr catalyst for isobutanol synthesis from syngas

Xiaofeng Gao [a,b], Yingquan Wu [a], Guohui Yang [a], Tao Zhang [a], Xiaoli Li [a,b], Hongjuan Xie [a], Junxuan Pan [a] and Yisheng Tan [a,c]*

[a] State Key Laboratory of Coal Conversion, Institute of Coal Chemistry, Chinese Academy of Sciences, Taiyuan 030001, China. Email: tan@sxicc.ac.cn. Fax: +86 351 4044287.Tel: +86 351 4044287.

[b] University of Chinese Academy of Sciences, Beijing 100049, China

[c] National Engineering Research Center for Coal-Based Synthesis, Institute of Coal Chemistry, Chinese Academy of Sciences, Taiyuan 030001, China

Graphical Abstract

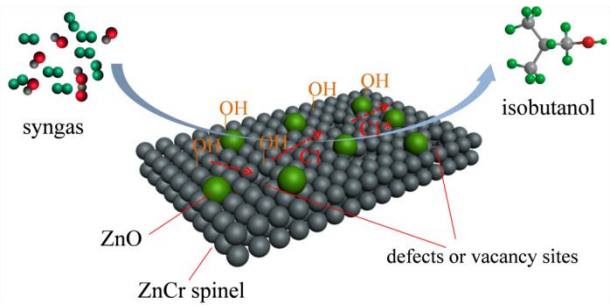

The hydroxyl groups could be consumed by CO under the interaction between ZnO and ZnCr spinel, resulting in more exposed oxygen vacancies for C-O activation.

Highlights

1. **ZnCr catalysts are prepared by sol-gel method to explore role of hydroxyl groups.**
2. **Lower calcination temperature causes more structure defects and hydroxyl groups.**
3. **The ZnCr prepared at pH=2 exhibits high total alcohol and isobutanol selectivity.**
4. **The hydroxyl groups could be consumed by CO, resulting in more oxygen vacancies.**

Abstract

A series of ZnO, ZnCr catalysts were prepared by a sol-gel method and ammonia solution. The catalysts were characterized by XRD, in-situ FR-IR, NH_3-TPD, in-situ XPS, HRTEM. The

results show that lower calcination temperature is helpful to reduce the crystal size and crystallinity of ZnCr nanocrystal, as well as forming a certain amount of structure defects and hydroxyl groups. The hydroxyl groups could be consumed by CO under the interaction between ZnO and ZnCr spinel, resulting in more exposed oxygen vacancies. We find the proper calcination temperature and Zn/Cr molar ratio for the ZnCr catalysts preparation are 400 ^{o}C and 1.0, respectively. The Zn_1Cr_1-400~2.0 catalyst prepared with the pH value of 2 shows more hydroxyl groups and small particle size, exhibiting the best catalytic performance both on the CO conversion (20.9%) and isobutanol selectivity (24.2 wt%).

Keywords: $ZnCr_2O_4$, ZnO, hydroxyl groups, interaction, oxygen vacancies

1. Introduction.

Syngas (CO + H_2), one of the most important industrial chemical products, is widely used as raw material for other chemicals synthesis or directly as fuel [1-4]. Syngas conversion to other chemicals, Fischer-Tropsch synthesis, methanol synthesis, etc., has attracted extensive attentions with the development of modern catalysis science. Among lots of processes for syngas conversion, the higher alcohols synthesis has been widely investigated due to its broader prospects in our society and huge market demand as fuel blends, additive agent or in intermediates for fine chemicals synthesis [5-9]. Isobutanol is one important alcohol product. It could be used directly as an additive to improve the quality of gasoline, on the other hand, it is also an essential intermediate material to produce antioxidants, plasticizer, synthetic rubber, esters, etc [10-12]. However, isobutanol is mainly obtained as the by-product of butanol

synthesis during propylene carbonyl reaction. This general isobutanol synthesis method is unable to meet the growing demand. Considering the increasing price of petroleum and the requirement of the environmental friendly policy, a low cost and non-oil route for isobutanol synthesis is necessary and has roused considerable research interests.

For isobutanol synthesis from syngas, recently, researchers mainly focus on three types catalysts: alkali-modified Cu-based methanol synthesis catalysts [13-15], and alkali-modified Cr-based methanol synthesis catalysts [16, 17] and ZrO_2 based catalyst [18]. The ZnCr nanospinel catalyst has been studied extensively since 1980s due to its high activity and selectivity for isobutanol synthesis at high-temperature and high-pressure. The products obtained over the ZnCr catalysts are mainly composed of methanol and isobutanol with a negligible amount of other components, which make the industrial-scale isobutanol synthesis from syngas possible. The mechanism of isobutanol synthesis from syngas on ZnCr catalyst is still not explicitly established. The catalyst active sites and the reaction mechanism are always the focus of researchers in the past years. Now, the majority debates of the active sites on ZnCr catalyst for isobutanol/methanol synthesis can be grouped into the following three explanations: (a) the excess ZnO modified by alkali metals on ZnCr spinel, (b) the non-stoichiometry phase (ZnCr) with cation disorder, (c) the oxygen vacancies on ZnCr based catalysts. Epling et al. [19-21] had reported that the ZnCr spinel was not important for isobutanol synthesis and acted only as a high-surface-area support. As the near-surface region contained primarily ZnO with very little Cr, thus they drew a conclusion that the alkali-modified ZnO phase was the active catalyst site. Meanwhile, they pointed out that the hydroxyl groups played an important role in the HAS (higher alcohol synthesis) reaction. Removal of hydroxyl groups could expose more of the active catalyst sites. Nevertheless, Piero et al. [22] reported that the non-stoicheiometric spinel-like phase (ZnCr)

must be the active sites for methanol synthesis from syngas at high temperature. An unusual co-ordination could be formed when the Zn atoms occupied the octahedral sites of ZnCr spinel, which facilitated methanol synthesis. There are also some other studies presenting the similar opinions [23,17]. In our previous studies, our group has performed a lot of works on the reaction mechanism and catalyst active sites for isobutanol synthesis from syngas. Wu et al. [24-26] indicated that COH→CCOH was the slow initial growth step for isobutanol synthesis on ZrO_2-based catalyst based on chemical enrichment method. The isobutanol was derived from the C_{2+} alcohols undergoing an aldo-condensation reaction at high temperature. Tian et al. [27-30] demonstrated that the non-stoichiometric spinel ($Zn_xCr_{2/3(1-x)}O$), presenting variation of cations on the tetrahedral and octachedral coordination sites, was the active catalytic sites for isobutanol formation. And the isobutanol productivity increased linearly with the increase of the cation disorder degree. In the recent years, more and more researchers consider the oxygen vacancies of ZnCr based catalysts are the active sites for methanol/isobutanol synthesis from syngas. The oxygen vacancies could improve the activation ability of C-O band on surface of different spinel, such as $ZnCr_2O_4$ [31], Fe_3O_4 [32], Cu/ZnO [33] and $ZnCa_2O_4$ [34]. Lunkenbein et al. [35] showed that the sintering of ZnO and the loss of oxygen vacancies caused a decrease in the catalytic activity of Cu-based catalysts for methanol synthesis.

Although the ZnO phase shows almost no catalytic activity for isobutanol synthesis, however, we found that the addition of ZnO phase could obviously enhance the catalytic performance of ZnCr spinel catalysts both in CO conversion and isobutanol selectivity. The similar results had also been reported by Kuld et al. for the methanol synthesis reaction over the ZnO promoted Cu catalysts [36], and they deemed that the improved catalyst performance was related to the Zn coverage and the size-dependent thermodynamic activities of the Cu and ZnO nanoparticles. Our

previous study [27] has proved that there exists interaction between ZnO and ZnCr spinel, but how the interaction works is not explicit. In order to further explore the roles of ZnO and ZnCr spinel for isobutanol synthesis from syngas, in this report we designed a series of ZnCr based catalysts via a sol-gel method, discovering the function of hydroxyl groups under the interaction between ZnO and ZnCr spinel. In addition, the chemical and physical properities of catalysts constructed by different preparation methods could significantly affect catalysts performance. Compared with the previous studies [27-31], in which the ZnCr nanospinel catalysts used for isobutanol synthesis are mainly prepared by co-precipitation method, the sol-gel method in this paper could achieve molecular level mixing which facilitates the formation of polycrystalline homogeneous particles with improved properties.

2. Experimental Method

2.1 Catalyst preparation.

All the catalysts were prepared by sol-gel method and the used chemicals were analytic grade. The pure ZnO was prepared by using $Zn(NO_3)_2 \cdot 6H_2O$ as precursor and oxalic acid as complexing agent. 59.5 g $Zn(NO_3)_2 \cdot 6H_2O$ was dissolved in 200 mL ethanol under vigorous stirring at 50^{o}C, and then 200 mL ethanol solution containing 29.0 g oxalic acid was added into the above solution by peristaltic pump with the flow rate of 20 mL/min under vigorous stirring. The obtained solution was aged for 20 h at room temperature to form a sol. Subsequently, the sol was directly heated at 70 ^{o}C for 2 h and 120 ^{o}C for another 10 h to evaporate the ethanol solvent to form a gel. Finally, the gel was calcined at 250 ^{o}C for 2 h to decompose the organic chemicals completely, followed by calcination at 400 ^{o}C for 6 h to obtain the pure ZnO sample.

We also prepared a series of ZnCr catalysts Zn_xCr_1-y (x=0.5; y=800, 600，400) and Zn_xCr_1-y (x=1, 1.5 or 3; y=400) by the similar method to the above ZnO catalysts preparation.

$Zn(NO_3)_2 \cdot 6H_2O$ and $Cr(NO_3)_3 \cdot 9H_2O$ were employed as Zn and Cr resources, respectively. The amount of oxalic acid is excess 15 mol% in order to ensure all the metal ions completely chelating with oxalic anion. After aging, evaporation of the ethanol solvent and calcination, the Zn_xCr_1-y (x=0.5; y=800, 600，400) and Zn_xCr_1-y (x=1, 1.5 or 3; y=400) catalysts were obtained, where the "x" in the catalyst name stands for Zn/Cr molar ratio, the "y" means ultima calcination temperature. As the Zn/Cr molar ratio was 0.5, only $ZnCr_2O_4$ phase formed. When the Zn/Cr molar ratio exceeded 0.5, besides $ZnCr_2O_4$ phase, the ZnO phase also formed.

For the sol-gel method, after the addition of oxalic acid ethanol solution into the metal nitrate solution, the pH value of the sol was less than 1. Since the pH value can influence the structure and morphology of the ZnCr catalysts, we used ammonia solution (28 wt%) to adjust the pH value of the sol, by which to get a series of ZnCr spinel catalysts. Required amount of ammonia solution was added to keep the pH value of the final sol solutionat 1.0, 2.0, 3.0 and 4.0. After aging, evaporation of the ethanol solvent and calcination, a series of catalysts (Zn/Cr=1.0, 400 ^oC) named Zn_1Cr_1-400~z were obtained, where the "z" denotes the pH value of sol solution.

All the catalysts were impregnated with potassium carbonate through an incipient wetness method to get the final 3 wt% K_2O promoted catalysts for isobutanol direct synthesis from syngas. The size of all the catalysts were in 30~40 mesh.

2.2 Catalytic performance measurement.

All the catalysts were first reduced with a 10% hydrogen-in-nitrogen mixture for 4 h at 400 ^oC on-line before reaction. Then, these catalysts were tested for isobutanol catalytic activity in a fixed bed using a feed gas of $CO:H_2$ = 2.6:1 at a space velocity of 3,000 h^{-1}. The reactions were performed at 400 ^oC and 10 MPa. Products were analyzed by four on-line GC during the reaction. Inorganic gas products of CO, H_2, CH_4 and CO_2 were detected on-line by thermal

conductivity detector using a GC4000A (carbon molecular sieves column). The organic gas products of hydrocarbons and methanol were detected on-line by flame ionization detector using a GC4000A (GDX-403 column). The alcohol products in liquid phase were detected by flame ionization detector using a GC-7AG (Chromsorb101). The H_2O and methanol products in liquid phase were detected by thermal conductivity detector using a GC4000A (GDX-401column).

2.3 Catalyst characterization.

The X-ray diffraction (XRD) data of the catalysts were collected using a D8 Advance X-ray diffractometer in a 2θ range from 10° to 80° with Cu Kα radiation. The morphology and microstructure of catalysts were investigated using a field emission transmission electron microscope (HRTEM, JEM-2100F) operated at 400kV. The (in-situ) XPS patterns were recorded using an AXIS ULTRA DLD X-ray photoelectron spectrometer equipped with a multichannel detector. Charge referencing was done against adventitious carbon (C 1s, 284.8 eV). A Shirley-type background was subtracted from the signals. The recorded spectra were fitted using Gauss–Lorentz curves to determine the surface composition of different samples. FT-IR Spectra were obtained with a TENSOR-27 in the range from 4000 to 600 cm^{-1} with 4 cm^{-1} resolution. In-situ IR Spectra of H_2 reduction were recorded by a TENSOR-27 from beginning introduction of hydrogen at 400 °C. In-situ IR Spectra of CO adsorption and desorption were obtained by a TENSOR-27 in the range from 600 to 4000cm^{-1} with 4 cm^{-1} resolution after H_2 reduction for 0.5 h at 400 °C on line. CO adsorption was taken at 400 °C and after 0.5 h of pure Ar flow at the same temperature and the adsorbates existing on the surface of different ZnCr spinel catalysts would be measured. The NH_3 Temperature Programmed Desorption (NH_3-TPD) was recorded on TP-5050 automatic chemical adsorption instrument in the range from 50°C to 600 °C. Pure standard mixtures (zeolite + activated carbon) were used during preliminary TPD measurements.

It was saturated with NH_3 flow at 50ºC after pretreatment at 400 ºC for 180 min in reducing gas of 10% H_2 in Ar. Then pure Ar flowed for 120 min at the same temperature to eliminate the adsorption of physically adsorbed water and impurities. Finally, the temperature was increased at a constant rate of 5ºC min^{-1} under an appropriate amount of Ar flow. The desorbed species were analyzed on GC4000A by thermal conductivity measurements. The chemical compositions of the catalysts were measured by inductively coupled plasma–atomic emission spectroscopy (ICP–AES) using a Thermo iCAP 6300 instrument.

3. Results and discussion.

The catalytic performance of ZnO, Zn_xCr_1-y and Zn_1Cr_1-400~z catalysts for isobutanol synthesis from syngas is shown in Table 1. The ZnO catalyst shows the CO conversion of 16.8%, but the selectivity for alcohol is only 21.6%. The main product of the alcohol is methanol (78.7 wt%) and only a little amount of isobutanol (2.9 wt%) is produced. Therefore, the alkali metal promoted ZnO is not a good catalyst candidate for isobutanol synthesis. For the $Zn_{0.5}Cr_1$-y (y=800, 600 or 400, $ZnCr_2O_4$ phase) catalysts, the selectivity of alcohol increases from 11.4% to 60.1% with decreasing the calcination temperature from 800 ºC to 400 ºC and the total alcohol production ratio also reaches a maximum value for $Zn_{0.5}Cr_1$-400 of 0.051 $g{\cdot}mL^{-1}{\cdot}h^{-1}$. Meanwhile, the weight percentage of isobutanol increases clearly from 1.6 wt% to 14.7 wt%. These data indicate that the catalyst with lower calcination temperature has better catalytic performance both on higher catalyst activity and higher isobutanol selectivity. As shown by the XRD patterns in Fig. 1 and HRTEM images in Fig. 2, the lower calcination temperature results in lower crystallinity and smaller particle size, which maybe contribute to the formation of defects or activity sites for the isobutanol synthesis from syngas. Because the reaction temperature of this

conversion process is 400 ºC, there is no point in decreasing the calcination temperature further.

If the Zn/Cr molar ratio in Zn_xCr_1-400 catalysts exceeds 0.5, the formation of ZnO phase can be confirmed clearly. Compared with $Zn_{0.5}Cr_1$-400 catalyst, the increased Zn/Cr molar ratio of 1.0 in Zn_1Cr_1-400 catalyst results in promoted CO conversion from 11.3% to 16.8% and enhanced isobutanol selectivity from 14.7 wt% to 20.9 wt%. It must be stressed that though the ZnCr spinel ($Zn_{0.5}Cr_1$-400) has a certain catalytic activity for isobutanol synthesis, its activity is substantially boosted by the interaction with ZnO (Zn_1Cr_1-400). The in-situ CO FT-IR in Fig. 6 and in-situ XPS in Fig. 9 have verified that the hydroxyl groups could be consumed by CO under the effect of synergy between ZnO and ZnCr spinel, whereby to increase the amount of oxygen vacancies for isobutanol synthesis from syngas. The $Zn_{1.5}Cr_1$-400 catalyst gives similar CO conversion and isobutanol selectivity to that of Zn_1Cr_1-400 catalyst, but lower total alcohol selectivity of 60.7%. Further increasing the Zn/Cr molar ratio to 3.0, however, results in a sharp decrease on isobutanol selectivity (11.8 wt%) and CO conversion (13.1%). Higher Zn/Cr molar ratio like 3.0 will decrease the amount of $ZnCr_2O_4$ phase in ZnCr catalyst, and the ZnO phase is the predominant component, therefore resulting in lower activity. The catalytic performance of ZnCr catalysts with varied Zn/Cr molar ratios is shown in Table S1and Fig. S1a.

In order to adjust the amount of hydroxyl groups and the interaction between ZnO and ZnCr spinel, ammonia solution (28 wt%) was used to change the pH value of the sol solution for Zn_1Cr_1-400~z catalysts preparation. Compared with Zn_1Cr_1-400 catalyst, the Zn_1Cr_1-400~1.0 and Zn_1Cr_1-400~2.0 catalysts show a great increase both in the CO conversion and the isobutanol selectivity. A maximum total alcohol production rate of 0.103 $g \cdot mL^{-1} \cdot h^{-1}$ is achieved at pH=2.0. Increasing the pH value to 4.0, however, results in a sharp decrease both on the total alcohol production rate and isobutanol selectivity. The catalytic performance of ZnCr catalysts

with varied pH value of sol solution is shown in Table S2 and Fig. S1b.

The stability of the Zn_1Cr_1-400~2.0 catalyst is further measured in Fig S2. The results demonstrate that the Zn_1Cr_1-400~2.0 catalyst shows excellent stability over 300 h on stream. The CO conversion could stably maintain at 22 ± 2 % and the total alcohol selectivity is only reduced by 4% throughout the test. In the first 160 h on stream, the weight percentage of isobutanol in liquid products keeps above 24 wt%, and slightly decreases in the rest of the test. Thus, the Zn_1Cr_1-400~2.0 catalyst is a suitable catalyst candidate for isobutanol synthesis directly from syngas.

The XRD patterns of different catalysts are presented in Fig. 1. The ZnO catalyst in Fig, 1a displays the typical peaks at 31.8°, 34.4°, 36.3°, 47.5°, 56.6° and 62.9° related to ZnO phase (JCPDS cards 36-1451), indicating that ZnO crystal formed well in the sol-gel method. For the catalysts of $Zn_{0.5}Cr_1$-400, $Zn_{0.5}Cr_1$-600 and $Zn_{0.5}Cr_1$-800 in Fig. 1a, only some typical peak appeared at 30.3°, 35.7°, 43.4°, 57.5° and 63.1°, which is ascribed to $ZnCr_2O_4$ (JCPDS cards 22-1107). It should be noted, here, the diffraction intensity of different catalysts is different. By decreasing the calcination temperature, the diffraction peaks become broader and the intensity decreases linearly, illustrating the smaller crystal particle size obtained at lower calcination temperature. In our previous study, we had proved that the calcination temperature employed for $ZnCr_2O_4$ spinel preparation greatly influenced the crystal structure [29, 30]. Lower calcination temperature would cause low crystallinity of $ZnCr_2O_4$ spinel, meanwhile, leading to serious cation disorder and more structure defects. This kind of $ZnCr_2O_4$ spinel with cation disorder was called non-stoichiometric spinel ($Zn_xCr_{2/3(1-x)}O$), as reported by other articles [37, 23]. The

particle size calculated by Scherrer equation decreases from 24.7 nm to 4.8 nm with decreasing the calcination temperature from 800 ºC to 400 ºC. The ZnCr spinel catalysts with excess ZnO, Zn_xCr_1-y (x=1.0, 1.5, 3.0; y=400), exhibit two kinds of typical diffraction peaks corresponding to $ZnCr_2O_4$ and ZnO respectively. Among these catalysts, the increasing trend of the intensity of ZnO diffraction peaks is more obvious with Zn/Cr molar ratio increasing from 1.0 to 3.0, however, the $ZnCr_2O_4$ diffraction peaks change little.

We also used ammonia solution to adjust the pH value of sol solution to get the catalysts with varied crystallinity. The XRD patterns of the prepared catalysts are shown in Fig. 1b. It is shown that the intensity of diffraction peaks of both ZnO and $ZnCr_2O_4$ phases is much lower as the pH value is in the range of 1~3. Accordingly, the ZnO and $ZnCr_2O_4$ particle size of Zn_1Cr_1-400~1.0, Zn_1Cr_1-400~2.0, Zn_1Cr_1-400~3.0 catalysts should be much smaller than those of Zn_1Cr_1-400~4.0 catalyst. By careful observation, the crystallinity of Zn_1Cr_1-400~2.0 is lowest among these catalysts. It is worth noting that there is no diffraction peaks of potassium species in the XRD pattern of all catalysts, indicating the potassium species would be amorphous or dispersed well so that they could not be detected by XRD.

The HRTEM was employed to characterize the morphology and microstructure of ZnO and Zn_xCr_1-y catalysts. The TEM images are shown in Fig. 2. The TEM images of ZnO catalyst in Fig. 2a show that the particles are well-separated, and the particles size is in the range of 20~60 nm, peaking at 30~40 nm, much bigger than that of other catalysts. For the $Zn_{0.5}Cr_1$-y catalysts in Fig. 2b-d, the mean particle sizes of $Zn_{0.5}Cr_1$-800, $Zn_{0.5}Cr_1$-600 and $Zn_{0.5}Cr_1$-400 catalysts are obtained as about 25 nm, 11 nm and 4.5 nm, respectively. This decline trend should be attributed to the lower calcination temperature, which is helpful to reduce the crystal size. Furthermore, the

typical lattice spacing of 4.81 Å, 2.95 Å, 2.51 Å, are corresponded to the (111), (220), (311) planes of $ZnCr_2O_4$ nanocrystal. ZnO phase is not observed as the Zn/Cr molar ratio is 0.5. If the Zn/Cr molar ratio exceeds 0.5 (Fig. 2e-g), the TEM images clearly demonstrate that, besides $ZnCr_2O_4$ nanocrystal, the ZnO phase also formed with a typical lattice spacing of 2.48Å corresponded to (101) plane of ZnO crystal. These results are in good agreement with XRD results in Fig. 1. It should also be noted that the particle size of ZnO on Zn_1Cr_1-400 catalyst is much smaller than pure ZnO sample in Fig. 1a that makes a close connection between ZnO and $ZnCr_2O_4$ phase and is helpful to improve the interaction between them. With increasing the Zn/Cr molar ratio from 1.0 to 3.0, the particle size of ZnO crystal increases obviously, but the particle size of $ZnCr_2O_4$ crystal changes slightly. For Zn_3Cr_1-400 catalyst, the amount of ZnO phase with the particle size in the range of 20~30 nm increases to be the predominant component of the sample. The aggregation degree of ZnO particles on this Zn_3Cr_1-400 catalyst is higher than other Zn_xCr_1-400 catalysts, finally resulting in poor catalytic performance both in CO conversion (13.1%) and isobutanol selectivity (11.8 wt%).

The TEM images of Zn_1Cr_1-400~z catalysts prepared with different pH value of sol solution are shown in Fig. 3. Compared with Zn_1Cr_1-400 catalyst in Fig. 2e, the TEM images of Zn_1Cr_1-400~z catalysts exhibit different morphology. As the pH value is in the range of 1~3, the particles are relative small and the smallest particle size is obtained at pH = 2 which is helpful to improve the isobutanol selectivity (24.2 wt%) for Zn_1Cr_1-400~2.0. Further increasing the pH value of sol solution can change the morphology of ZnO and $ZnCr_2O_4$ crystal at the same time. For Zn_1Cr_1-400~4.0 catalysts, the morphology and particle size of ZnO and $ZnCr_2O_4$ increase clearly. It could be easily observed that the ZnO phase and the $ZnCr_2O_4$ phase separate from each other with a particle size in the range of 20~50 nm when the pH value is 4 (Fig. 3d). The

poor catalytic performance of Zn_1Cr_1-400~4.0 in CO conversion (13.0%) and isobutanol selectivity (4.6 wt%) should be contributed to the high crystallinity and poor interaction between ZnO and $ZnCr_2O_4$.

The FT-IR spectrum of ZnO, Zn_xCr_1-y and Zn_1Cr_1-400~z catalysts is shown in Fig. 4. The broad band at around 3480 cm^{-1} should be attributed to the H-O band vibration modes of hydroxyl groups [38-41]. For the ZnO catalyst, the amount of hydroxyl groups is more than other catalysts. It is clear that, with the decrease of calcination temperature from 800 ºC to 400 ºC, the FT-IR bands of H-O vibration modes of the $ZnCr_2O_4$ spinel catalysts increase obviously. As the cation disorder could be more serious at low calcination temperature, the Zn^{2+} ions are located in octahedral sites in a random substitution of Cr^{3+}ions, leaving some of the tetrahedral vacant sites [22]. Then, the oxygen atoms around theses vacant sites would tend toward to form hydroxyl groups. Additionally, increasing the Zn/Cr molar ratio of Zn_xCr_1-400 catalyst from 0.5 to 3.0 further increases the content of hydroxyl groups. This fact might be explained by the formation of ZnO phase on the surface of ZnCr spinel, which is consistent with the X-ray diffraction results in Fig. 1. As the ammonia solution (28wt%) is used to adjust the pH value of sol solution, the intensity of H-O band vibration modes become stronger at pH =2 and 3 and weaker at other pH values. Especially, as the pH value of the sol solution is 4, the amount of hydroxyl groups of Zn_1Cr_1-400~4.0 catalyst is much less than that of other catalysts.

The band at 1637 cm^{-1} is assigned to the surface adsorbed oxygen species (O_{ads}) [42, 43]. We found that the non-stoichiometric spinel with disordered cations was not stable [28]. Large numbers of dangling bonds (O_{ads}+ O_{OH}^-) existing in the surface of Zn_xCr_1-400 and Zn_xCr_1-400~z catalysts would stabilize this metastable state. However, the band signals at 1637 cm^{-1} for $Zn_{0.5}Cr_1$-800 and Zn_1Cr_1-400~4.0 catalysts are hardly observed, because the high calcination

temperature and high pH value of sol solution cause the catalysts with higher crystallinity. This result also led to the low reaction activity of $Zn_{0.5}Cr_1$-800 and Zn_1Cr_1-400~4.0 catalysts during the reaction of isobutanol synthesis from syngas as shown in Table 1. The band at 1380 cm^{-1} and 830 cm^{-1} should be assigned to NO_3^- ion that originated from nitrate precursor [44-46]. The band at 1100 cm^{-1} corresponded to O=C=O vibration is derived from oxalate precursor [38, 39]. For $Zn_{0.5}Cr_1$-800 catalyst, the bands related to NO_3^- ion and O=C=O vibration are much weaker than other catalysts, suggesting that the residues from precursor materials for this catalyst preparation had been removed completely by high temperature calcination. The broad peak near 940 cm^{-1} should be assigned to the deformation mode of Zn-O at 945 cm^{-1} merged with the band of Cr^{6+} at 935 cm^{-1} [47]. The band at 1583 cm^{-1} is ascribed to the asymmetric stretching vibration of C=O mode [45], which is only observed for ZnO catalyst.

The acidic properties of the catalysts were evaluated by NH_3-TPD. The profiles are shown in Fig. 5. and the acid sites distribution is shown in Table S3. The acidity pattern shows that there are two main types of desorption peaks on catalysts, indicating two kinds of acid sites: a large amount of weak acid sites and a small amount of strong acid sites in range of 150 ~ 300 ^oC and 400 ~ 550 ^oC respectively. For ZnO and $Zn_{0.5}Cr_1$-800 catalysts, the amount of both weak and strong acid sites is small, even hardly being detected. But by decreasing calcination temperature, the amount of weak acid sites of ZnCr spinel (Fig. 5b-d) significantly increases and a certain amount of strong acid sites appear. When the Zn/Cr molar ratio exceeds 0.5 (Fig. 5d-g), the area of weak acid sites increases and the peak becomes wide. Meanwhile, the low temperature peaks shifts towards higher temperature, but the strong acid peaks do not change obviously. Hoflund et al. [48] had used Mn atom to replace a part of Cr atom in ZnCr spinel. Since the acidity of Mn is

weaker than that of Cr, the catalyst showed low hydrocarbon selectivity. In our study [29], we have found that the existed weak acid sites is beneficial to improve the catalytic activity for the isobutanol synthesis from syngas, on the contrary, the strong acid sites on the catalysts would depress the formation of alcohol and isobutanol.

Fig. 5h-k shows the acidic properties of ZnCr catalysts prepared with the sol solution that had been adjusted on its pH value. Compared with Zn_1Cr_1-400~1.0, the amount of both weak acid sites and strong acid sites of Zn_1Cr_1-400~2.0 catalyst increase obviously, but further increasing pH value leads to smaller acid site amount, even no acid peaks for Zn_1Cr_1-400~4.0. As the results shown in Table S3, the amount of weak acid sites reaches a maximum of 40.59 umol/g at pH=2.0. It is worth noting that the weak acid peaks of Zn_1Cr_1-400~z catalysts shift to lower temperature with increasing the pH value, indicating that the intensity of weak acid sites become weaker. The proper acidic properties of Zn_1Cr_1-400~2.0 may be an important reason for its high alcohol yield during the isobutanol synthesis.

The in-situ CO FT-IR was employed to detect the change of species after adsorbing CO molecule at 400 ^oC, and the result profiles are shown in Fig. 6. The inversus peak at 3480 cm^{-1} shows the consumption of hydroxyl groups, and the bands at 1560 cm^{-1} and 1375 cm^{-1} correspond to the vibration of $\nu_{as}(CO_3^-)$ and σ(CH) originating from formate species [49, 50]. The peak at 1330 cm^{-1} could be attributed to the carbonate species [49, 50]. For the ZnO catalyst, only a little amount of formate species formed after adsorbing CO molecule. For the $Zn_{0.5}Cr_1$-y catalysts (Fig. 6b-d), a large number of formate and carbonate species are produced by calcination from 800 ^oC to 400 ^oC. In general, the formate species is considered as an important intermediate for alcohol synthesis. Waugh et al. [51] had found that the formate species was a stable intermediate during the conversion of CO/CO_2 to methanol, while the carbonate species

was not essential to alcohol synthesis beacuse it was easily converted to CO_2. Tian [28, 30] and Wu [26] reported that the formate species was a very significant C1 intermediate for isobutanol from syngas and its formation was associated with consuming hydroxyl groups and adsorbed CO on catalyst surface. In this study, however, formate species could be formed on the $Zn_{0.5}Cr_1$-y catalysts without consuming hydroxyl groups, although there is a certain amount of hydroxyl group verified by FT-IR spectrum in Fig. 4.

It needs to be stressed that, though a large amount of formate species are formed for the $Zn_{0.5}Cr_1$-800 catalyst, its catalytic activity is much lower than others as shown in Table 1. This means that besides the formate species (one C1 intermediate), there must exist another C1 intermediate (denoted as C1*) which is difficult to be formed for the catalysts calcinated at high temperature. With decreasing calcination temperature from 800 ^oC to 400 ^oC, the isobutanol distribution in the liquid products of $Zn_{0.5}Cr_1$-y catalysts increases from 1.6 wt% to 14.7 wt%. A lot of defects and oxygen vacancies will exist on catalyst surface at lower calcination temperature that may be essential to the formation of C1* intermediate.

Fig. 6d-g shows the in-situ CO FT-IR analysis results of Zn_xCr_1-400 catalysts as the Zn/Cr molar ratio increases from 0.5 to 3.0. For Zn_1Cr_1-400, the carbonate species signal at 1300 cm^{-1} gets minimized among the Zn_xCr_1-400 catalysts. However the signal of formate species at 1560 cm^{-1} increased slightly with increasing the Zn/Cr molar ratio. For the inversus peak of hydroxyl groups consumption at 3480 cm^{-1}, an obvious hydroxyl consumption peak formed when the Zn/Cr molar ratio exceeds 0.5, suggesting that the interaction between ZnO and ZnCr spinel could improve the utilization of hydroxyl species. Moreover, the Zn_1Cr_1-400 shows the biggest hydroxyl consumption peak compared with other Zn_xCr_1-400 catalysts. The interaction between ZnO and ZnCr spinel, possibly, was more effective or stronger when the Zn/Cr molar ratio is 1.0.

As the reaction results exhibited in Table 1, the Zn_1Cr_1-400 gives excellent catalytic performance, with total alcohol production rate of 0.098 $g \cdot mL^{-1} \cdot h^{-1}$ and isobutanol distribution of 20.9 wt%, better than other Zn_xCr_1-400 catalysts. Epling et al. [19-21, 52, 53] showed that the hydroxyl groups could interact with or cover the active catalytic sites in the near-surface region, and the reductive pretreatment preformed on the catalysts before reaction in HAS (higher alcohol synthesis) reactor resulted in the removal of hydroxyl groups, thereby exposing more of the active catalyst sites. Bao and his co-wokers [31] reported that Density functional Theory (DFT) calculations using the $ZnCr_2O_4$ spinel (111) surface as a model revealed that it was reductive, resulting in a surface with a number of oxygen vacancies. Meng et al [54] found that the enrichment of the acid sites could be related to the formation of oxygen vacancy by the reduction of MoO_3 and V_2O_5. Other studies had also reported that the oxygen vacancies could improve the activation ability of C-O bond on surface of different spinels, for example Fe_3O_4 [32], Cu/ZnO [33] and $ZnCa_2O_4$ [34]. The hydroxyl groups are not conducive to isobutanol synthesis, and removing them would lead to the exposure of oxygen vacancies. The in-situ H_2 reduction FT-IR of Zn_1Cr_1-400 was also employed and the spectrum is shown in Fig. S3. The results reveal that, although the catalysts are reduced by a 10% hydrogen-in-nitrogen mixture for 4 h at 400ºC before reaction, this reductive pretreatment could not remove the hydroxyl groups. On the contrary, the amount of hydroxyl groups increases.

From the discussion above, some conclusions could be drawn cautiously that the amount of hydroxyl groups increases with the formation of the non-stoichiometric spinel (calcinated at low temperature) and the hydroxyl groups could be removed by CO under the synergy between ZnO and ZnCr spinel to form more oxygen vacancies at reaction conditions. Except of formate species as a C1 intermediate, another one C1 intermediate (denoted as C1*) exist potentially for

isobutanol synthesis from syngas. The formation of this new C1* is closely related with the amount of oxygen vacancies and the interaction between ZnO and ZnCr spinel. Further investigation on uncovering this new intermediate of C1* should be performed in future study.

For the Zn_1Cr_1-400~z catalysts shown in Fig. 6h-k, the inversus peaks of hydroxyl group consumption decrease with increasing the pH value of sol solution from 1.0 and 2.0 to 3.0 and 4.0, and the carbonate species peaks shows similar tendency. While, the signal of formate species gets maximized at pH at 2.0. Isobutanol synthesis from syngas is not determined by one factor, as we known, and both of the oxygen vacancies and formate species play important roles in this process. Adjusting of pH value of sol solution for catalyst preparation could change the crystallinity and particle size of both ZnO and $ZnCr_2O_4$ spinel (Fig.1b and Fig.3), whereby to influence the interaction between them and the amount of hydroxyl groups. The analysis results here showed that the optimal pH value of sol solution is 2.0.

The x-ray photoelectron spectrometer was employed to characterize the composition of the near-surface region of Zn_xCr_1-y and Zn_1Cr_1-400~z catalysts and the results are shown in Fig. S4. Epling and his co-workers [52, 53] have reported that Zn is rich, but Cr is not, in the near-surface region of ZnCr catalysts. They drew the conclusion that the alkali-promoted ZnO was the active phase for HAS, and the ZnCr spinel only acted as a high-surface-area support. But in this study, it shows that the predominant peaks corresponded to Zn, O and Cr are readily distinguished in Fig. S4, and small amount of K features could be also observed. A clear change is about the Zn features that become bigger with increasing the Zn/Cr molar ratio. The Zn 2p and Cr 2p XPS analysis results of the fresh Zn_xCr_1-y and Zn_1Cr_1-400~z catalysts are shown in Fig. 7. The

binding energy of Zn 2p at 1022.2 eV and 1045.2 eV should be attributed to Zn^{2+} from ZnO and $ZnCr_2O_4$ spinel [28, 55]. The binding energy of Cr 2p at 576.4 eV and 586.0 eV are derived from Cr^{3+} of $ZnCr_2O_4$ spinel [28, 55, 56]. For the $Zn_{0.5}Cr_1$-y catalysts (y=800, 600 or 400), the binding energy of Zn $2p^{3/2}$ constantly increases with decreasing the calcination temperature from 800 °C to 400 °C. This change is due to the decrease of electron density of Zn cation in $ZnCr_2O_4$ spinel [57], which verifies that the cation disorder is more serious and more defects or oxygen vacancies could be formed for the catalyst prepared by lower calcination temperature. With the Zn/Cr molar ratio increasing from 0.5 to 3.0, the amount of ZnO phase increases and the binding energy of Zn $2p^{3/2}$ decreases. For the Zn_1Cr_1-400~z catalysts (z=1.0, 2.0, 3.0 or 4.0), the Zn $2p^{3/2}$ binding energy of Zn_1Cr_1-400~2.0 is higher than other catalysts, which may be owing to the stronger interaction between ZnO and $ZnCr_2O_4$ phase at pH =2.0. The binding energy of Cr 2p of different catalysts exhibits similar tendency with Zn 2p. The spectrum also shows a Cr^{6+} peak at 578.2 eV, indicating that the catalyst probably has been over oxidized.

The O 1s XPS analysis results of the fresh Zn_xCr_1-y and Zn_1Cr_1-400~z catalysts is shown in Fig. 8. The main chemical state of O in the near-surface region of all the catalysts is the lattice oxygen at 529.4 eV contributed by ZnO and $ZnCr_2O_4$ spinel [55, 56]. The O of hydroxyl species at 531.7 eV are derived from surface hydroxyl groups [58, 59]. The molar ratio of $(O_{OH^-})/(O_{latt} + O_{OH^-})$ obtained by quantitative calculation on the corresponding peaks areas is shown in Table 2. For the Zn_xCr_1-y (x=0.5; y=800, 600 or 400) catalyst, the molar ratio of $(O_{OH^-})/(O_{latt} + O_{OH^-})$ increases from 12.37 % to 19.14 % along with decreasing the calcination temperature from 800 °C to 400 °C. Because the ZnCr spinel (by low calcination temperature) with defect sites and cations disorder is unstable, more hydroxyl groups as dangling bonds are formed to stabilize this

metastable state. Varying the Zn/Cr molar ratio for Zn_xCr_1-y (x=0.5, 1.0, 1.5 or 3.0; y=400) catalysts preparation, obvious changes on the molar ratio of $(O_{OH^-})/(O_{latt} + O_{OH^-})$ have also been found. The hydroxyl groups signal increases when the Zn/Cr molar ratio is increased from 0.5 to 1.5, which is consistent with the FT-IR results in Fig. 4. For the Zn_3Cr_1-400 catalyst, a certain amount of chemisorbed O is observed at 526.6 eV, as reported by previous studies [19, 52, 53], which may be related to the chemical absorption on ZnO phase. Because the chemisorbed O could be eliminated by the H_2 reductive pretreatment preformed on the catalysts before the reaction [19, 53], so it is helpless for the isobutanol synthesis. For Zn_1Cr_1-400~z catalysts, the amount of hydroxyl groups has a maximum amount at pH=2 ($O_{OH^-}/(O_{latt} + O_{OH^-})$ = 25.52 %). Thus more oxygen vacancies could be formed for Zn_1Cr_1-400~2.0 catalyst after the introduction of CO at reaction temperature. A lowest value of $O_{OH^-}/(O_{latt} + O_{OH^-})$ appears on the Zn_1Cr_1-400~4.0, possibly due to the high crystallinity of both ZnO and $ZnCr_2O_4$ obtained with the pH value of 4.0.

The in-situ H_2 reduction and in-situ CO O 1s XPS spectrum of Zn_1Cr_1-400 catalyst at reaction temperature is shown in Fig.9, and the molar ratio of $(O_{OH^-})/(O_{latt} + O_{OH^-})$ is shown in Table 2. The in-situ H_2 reduction O 1s XPS in Fig. 9b shows the amount of hydroxyl groups increases apparently, which is consistent with the results of in-situ H_2 reduction FT-IR in Fig. S3. Nevertheless, the amount of hydroxyl groups significantly decreases with the introduction of CO at reaction temperature as indicated by Fig. 9c. These results indicate that the hydroxyl groups could not be consumed by the H_2 pretreatment, and they could react with CO under the interaction between ZnO and ZnCr spinel, which is consistent with the results of in-situ CO FT-IR in Fig. 6. Untill now, there is no an effective quantitative analysis tool to measure the oxygen vacancies on the surface of oxide catalyst during the reaction process. Therefore, the

surface compositions of Zn_1Cr_1-400 obtained by in-situ XPS analysis under different treatment conditions in Table 3 are employed to indirectly analyze the change of surface O amount on the ZnCr catalyst. It can be observed that the surface predominant elements of Zn, O, Cr and K change little after the H_2 treatment compared with fresh Zn_1Cr_1-400. However, the surface molar ratio of O decreases from 51.97 % to 48.14 % with CO introduction after H_2 pretreatment at 400 ^oC for 2 h. This phenomenon verifies that hydroxyl groups could be removed by CO, consequently resulting in more exposed oxygen vacancies to improve the catalyst performance. In addition, the molar ratio of Cr and K increases slightly after CO treatment, which should be attributed to that the alkali metal is bound to Cr under reduction treatment [60].

The bulk compositions of Zn_1Cr_1-400, Zn_1Cr_1-400~2.0 and used Zn_1Cr_1-400~2.0 catalysts (Zn, Cr, K) measured using inductively coupled plasma–atomic emission spectroscopy (ICP–AES) are presented in Table S4. The results show that the element compositions of Zn_1Cr_1-400, Zn_1Cr_1-400~2.0 catalyst are in agreement with recipe calculated from the element concentration presented in the synthetic solution. This means that the expected Zn/Cr molar ratio could be realized by sol-gel method with directly evaporating the ethanol solvent. For Zn_1Cr_1-400 catalyst, compared with surface composition in Table 3, the Zn/Cr molar ratio in bulk is a little higher than that at surface. The used Zn_1Cr_1-400~2.0 catalyst exhibits the similar element compositions to the fresh Zn_1Cr_1-400~2.0 catalyst that may be the main reason for its excellent stability (Fig S2).

The proposed mechanism of isobutanol synthesis is shown in Fig. 10. Based on the XRD and HRTEM analysis results, a relative perfect crystal could be formed when the ZnCr spinel is calcined at high temperature of 800 ^oC; meanwhile, the particle size is much bigger than other catalysts. Decreasing the calcination temperature could lead to small crystal particle size and low

crystallinity. On the other hand, lower calcination temperature will also cause the formation of structure defects including inherent oxygen vacancies. This kind of ZnCr spinel with cation disorder is also called non-stoichiometric spinel ($Zn_xCr_{2/3(1-x)}O$) that usually is in unstable state. Then, the oxygen atoms around the vacant sites and structure defects would tend to form hydroxyl groups to stabilize the metastable state, as proved by the FT-IR results (Fig. 4) that the amount of hydroxyl groups increases with decreasing the calcination temperature. The in-situ H_2 reduction FT-IR (Fig. S3) and in-situ H_2 reduction XPS (Fig. 9b) reveal that the H_2 pretreatment before the reaction could not remove the hydroxyl groups, on the contrary, the amount of hydroxyl groups increases with H_2 introduction. As the hydroxyl groups could interact with or cover the active catalytic sites, removing hydroxyl groups is helpful to expose these active sites in the near-surface region of catalysts. According to the results of in-situ CO FT-IR in Fig. 6 and the in-situ CO XPS in Fig. 9c, the hydroxyl groups could be consumed by CO molecule, resulting in the increase of surface oxygen vacancies for C-O activation. And the interaction between ZnO and ZnCr spinel could improve the utilization of hydroxyl groups. That may be one important reason why the activity of ZnCr spinel (by low calcination temperature) could be boosted by the interaction with ZnO for isobutanol synthesis, though the ZnO phase shows almost no catalytic activity. Because the formate species could be easily formed (Fig. 6b), we could draw a conclusion that there must exist another intermediate C1* whose formation is related to the oxygen vacancies. But what the intermediate C1* is needs to be further investigated in future study. The oxygen vacancies could be regenerated at the actual operation conditions, which is very important to obtain a long catalyst lifetime for the ZnCr based catalysts during the process of isobutanol synthesis from syngas [31]. A proposed pathway of isobutanol synthesis is shown in Fig. S5. The C1→C2 process is rate-determining-step for isobutanol

synthesis with coupling of two C1 intermediates [25, 61-64,]. After the C_2 alcohol is formed, the isobutanol could quickly synthesis by aldo-condensation reaction of C_{2+} alcohols [65, 66]. As stereo-hindrance effect is stronger for side reactions, the products obtained over the ZnCr catalysts are mainly composed of methanol and isobutanol with a negligible amount of other components [25].

Conclusion.

In this study, a series of ZnO, Zn_xCr_1-y and Zn_xCr_1-y~z catalysts were prepared by sol-gel method. With decreasing the calcination temperature for catalyst preparation, the crystallinity of $ZnCr_2O_4$ became lower with a certain amount of structure defects (including oxygen vacancies), and the particle size of catalysts also decreased obviously from the TEM images. Meanwhile, the amount of hydroxyl groups increased according to the FI-IR and XPS analysis results. The hydroxyl groups could be consumed by CO instead of H_2 under the interaction between ZnO and ZnCr spinel. Removing hydroxyl groups was helpful to expose more oxygen vacancies (the active sites for C-O activation). For the reaction of isobutanol synthesis directly from syngas, besides formate species (an important C1 intermediate), there must exist another intermediate C1* whose formation was closely related to the oxygen vacancies. The proper calcination temperature and Zn/Cr molar ratio for ZnCr catalysts preparation to realize efficient isobutanol synthesis from syngas were 400 ^oC and 1.0, respectively. Varied pH value of sol solution for catalyst preparation could obviously affect the amount of hydroxyl groups and nanocrystal morphology of the obtained ZnCr catalysts. The Zn_1Cr_1-400~2.0 catalyst (the pH value of sol solution is 2.0) showed more hydroxyl groups and a relative small particle size of ZnO and $ZnCr_2O_4$, realizing excellent interaction between ZnO and ZnCr spinel, whereby to exhibit the best catalytic performance for isobutanol synthesis from syngas: the CO conversion of 20.9%

and the isobutanol selectivity of 24.2 wt%.

Conflict of interest

The authors declare no competing financial interest.

Acknowledgements

This work was supported by the National Natural Science Foundation of China (21573269); The Key Research and Development Program of Shanxi Province, Special Research Foundation of Shanxi Province for Coal-based Synthesis of Fine Chemicals.

Notes and references

[1] I. Wender, Fuel Process. Technol. 48 (1996) 189-297.

[2] Y. Xiang, V. Chitry, P. Liddicoat, P. Felfer, J. Cairney, S. Ringer, N. Kruse, J. Am. Chem. Soc. 135 (2013) 7114-7117.

[3] H. M. Torres Galvis, K. P. de Jong, Acs Catal. 3 (2013) 2130-2149.

[4] V. Navarro, M. A. van Spronsen, J. W. M. Frenken, Nat. Chem. 8 (2016) 929-934.

[5] A. J. Medford, A. C. Lausche, F. Abild-Pedersen, B. Temel, N. C. Schjødt, J. K. Nørskov, F. Studt, Top. Catal. 57 (2014) 135-142.

[6] V. Subramani, S. K. Gangwal, Energy & Fuels 22 (2008) 814-839.

[7] J. G. Nunan, C. E. Bogdan, K. Klier, K. J. Smith, C.W. Young, R. G. Herman, J. Catal. 116 (1989) 195-221.

[8] J. Anton, J. Nebel, H. Song, C. Froese, P. Weide, H. Ruland, M. Muhler, S. Kaluza, J. Catal. 335 (2016) 175-186.

[9] X. Mo, Y.-T. Tsai, J. Gao, D. Mao, J. G.Goodwin Jr, J. Catal. 285 (2012) 208-215.

[10] L. Yu, S. Huang, S. Zhang, Z. Liu, W. Xin, S. Xie, L. Xu, Acs Catal. 2 (2012) 1203-1210.

[11] J. D. Taylor, M. M. Jenni, M. W. Peters, Top. Catal. 53 (2010) 1224-1230.

[12] G. Busca, Chem. Rev. 107 (2007) 5366-5410.

[13] N.-Y. Topsøe, H. Topsøe, J. Mol. Catal. A-Chem. 141 (1999) 95-105.

[14] J. G. Nunan, C. E. Bogdan, K. Klier, K. J. Smith, C.-W. Young, R. G. Herman, J. Catal. 113 (1988) 410-433.

[15] M. Xu, E. Iglesia, J. Catal. 188 (1999) 125-131.

[16] W. Keim, W. Falter, Catal. Lett. 3 (1989) 59-63.

[17] L. Tan, G. Yang, Y. Yoneyama, Y. Kou, Y. Tan, T. Vitidsant, N. Tsubaki, Appl. Catal. A-Gen. 505 (2015) 141-149.

[18] D. He, Y. Ding, H. Luo, C. Li, J. Mol. Catal. A-Chem. 208 (2004) 267-271.

[19] W. S. Epling, G. B. Hoflund, W. M. Hart, D. M. Minahan, J. Catal. 169 (1997) 438-446.

[20] G. B. Hoflund, W. S. Epling, D. M. Minahan, Catal. Lett. 45 (1997) 135-138.

[21] D. M. Minahan, W. S. Epling, G. B. Hoflund, Appl. Catal. A-Gen. 166 (1998) 375-385.

[22] G. D. Piero, F. Trifiro, A. Vaccari, Chem. Commun. (1984) 656-658.

[23] E. Errani, F. Trifiro, A. Vaccari, M. Richter, G. Del Piero, Catal. Lett. 3 (1989) 65-72.

[24] Y. Wu, H. Xie, Y. Kou, L. Tan, Y. Han, Y. Tan, J. Fuel Cell Sci. Technol. 41 (2013) 868-874.

[25] Y. Wu, H. Xie, Y. Kou, N. Tsubaki, Y. Han, Y. Tan, Korean J. Chem. Eng. 32 (2015) 406-412.

[26] Y. Wu, H. Xie, S. Tian, N. Tsubaki, Y. Han, Y. Tan, J. Mol. Catal. A-Chem. 396 (2015) 254-260.

[27] S. Tian, L. Tan, Y. Wu, Y. Kou, H. Xie, N. Tsubaki, Y. Tan, Appl. Catal. A-Gen. 536 (2017)

57-66.

[28] S. Tian, S. Wang, Y. Wu, J. Gao, P. Wang, H. Xie, G. Yang, Y. Han, Y. Tan, Catal. Sci. Technol. 6 (2016), 4105-4115.

[29] S. Tian, S. Wang, Y. Wu, J. Gao, Y. Bai, P. Wang, H. Xie, Y. Han, Y. Tan, J. Mol. Catal. A-Chem. 404–405 (2015) 139-147.

[30] S. Tian, S. Wang, Y. Wu, J. Gao, H. Xie, X. Li, G. Yang, Y. Han, Y. Tan, RSC Adv. 5 (2015) 89273-89281.

[31] F. Jiao, J. Li, X. Pan, J. Xiao, H. Li, H. Ma, M. Wei, Y. Pan, Z. Zhou, M. Li, S. Miao, J. Li, Y. Zhu, D. Xiao, T. He, J. Yang, F. Qi, Q. Fu, X. Bao, Science 351 (2016) 1065-1068.

[32] Y. Tamaura,; M. Tahata, Nature 346 (1990) 255-256.

[33] J. Xiao, T. Frauenheim, J. Phys. Chem. Lett. 3 (2012) 2638-2642.

[34] C. Jia, W. Fan, X. Cheng, X. Zhao, H. Sun, P. Li, N. Lin, Phys. Chem. Chem. Phys. 16 (2014), 7538-7547.

[35] T. Lunkenbein, F. Girgsdies, T. Kandemir, N. Thomas, M. Behrens, R. Schlögl, E. Frei, Angew. Chem.-Int. Edit. 128 (2016) 12900-12904.

[36] S. Kuld, M. Thorhauge, H. Falsig, C. F. Elkjær, S. Helveg, I. Chorkendorff, J. Sehested, Science 352 (2016) 969-974.

[37] S. Chen, Y. Wu, P. Cui, W. Chu, X. Chen, Z. Wu, J. Phys. Chem. C 117 (2013) 25019-25025.

[38] X. Kong, X. Zhang, J. Chen, Catal. Commun. 65 (2015) 46-50.

[39] L. Shi, Tan, Y. N. Tsubaki, ChemCatChem 4 (2012) 863-871.

[40] H. Li, J. Wang, H. Liu, C. Yang, H. Xu, X. Li, H. Cui, Vacuum 77 (2004) 57-62.

[41] R. Wahab, S. G. Ansari, Y.-S. Kim, H.-K. Seo, H.-S. Shin, Appl. Surf. Sci. 253 (2007)

7622-7626.

[42] Z.-X. Wei,; L. Wei,; L. Gong,; Y. Wang, C.-W. Hu, J. Hazard. Mater. 177 (2010) 554-559.

[43] L. Wu, J. C. Yu, L. Zhang, X. Wang, S. Li, J. Solid State Chem. 177 (2004) 3666-3674.

[44] Z. Yue, L. Li, J. Zhou, H. Zhang, Z. Gui, Mater. Sci. Eng. B 64 (1999) 68-72.

[45] X. L. Cheng, H. Zhao, L. H. Huo, S. Gao, J. G. Zhao, Sens. Actuator B-Chem. 102 (2004) 248-252.

[46] L. Shi, K. Tao, R. Yang, F. Meng, C. Xing, N. Tsubaki, Appl. Catal. A-Gen. 401 (2011) 46-55.

[47] A. Venugopal, R. Sarkari, S. N. Kumar, M. K. Kumar, S. S. John, J. K. Reddy, A. H. Padmasri, J. Chem. Sci. 126 (2014) 387-393.

[48] G. B. Hoflund, W. S. Epling, D. M. Minahan, Catal. Lett. 62 (1999) 169-173.

[49] A. Riva, F. Trifiro, A. Vaccari, L. Mintchev, G. Busca, J.Chem. Soc. Faraday Transactions 1: Physical Chemistry in Condensed Phases 84 (1988) 1423-1435.

[50] K. Pokrovski, K. T. Jung, A. T. Bell, Langmuir 17 (2001) 4297-4303.

[51] K. C.Waugh, Catal. Lett., 142 (2012) 1153-1166.

[52] W. S. Epling, G. B. Hoflund, D. M. Minahan, React. Kinet. Catal. Lett. 67 (1999) 225-232.

[53] W. S. Epling, G. B. Hoflund, J.Catal. 172 (1997) 13-23.

[54] Y. Meng, T. Wang, S. Chen, Y. Zhao, X. Ma, J. Gong, Appl. Catal. B-Environ. 160–161 (2014) 161-172.

[55] D. Gingasu, I. Mindru, D. C. Culita, L. Patron, J. M. Calderon-Moreno, Preda, S. O. Oprea, P. Osiceanu, E. Morena Pineda, Mater. Res. Bull. 49 (2014) 151-159.

[56] S. A. Hosseini, M. C. Alvarez-Galvan, J. L. G. Fierro, A. Niaei, D. Salari, Ceram. Int. 39 (2013) 9253-9261.

[57] Z. Zhang, Q. Zhang, L. Jia, W. Wang, T. Zhang, Y. Han, N. Tsubaki, Y. Tan, Catal. Sci. Technol. 6 (2016) 2975-2983.

[58] N. Liu, Z. Yuan, C. Wang, S. Wang, C. Zhang, S. Wang, Fuel Process. Technol. 89 (2008) 574-581.

[59] H. Zhao, P. Jiang, Y. Dong, M. Huang, B. Liu, New J. Chem. 38 (2014) 4541-4548.

[60] D. M. Minahan, W. S. Epling, G. B. Hoflund, J. Catal. 179 (1998) 241-257.

[61] R. M. Agny, C. G. Takoudis, Ind. Eng. Chem. Res. 24 (1985) 50-55;

[62] J. Saussey, J. C. Lavalley, J. Mol. Catal. 50 (1989) 343-353.

[63] S. Fujita, M. Usui, H. Ito, N. Takezawa, J. Catal. 157 (1995) 403-413

[64] K. C. Waugh, D. A. Whan, J. Chem. Soc.-Faraday Trans. 83 (1987) 2193-2212.

[65] K. J. Smith, R. B. Anderson, Can. J. Chem. Eng. 61 (1983) 40-45.

[66] K. J. Smith,; R. B. Anderson, J. Catal. 85 (1984) 428-436.

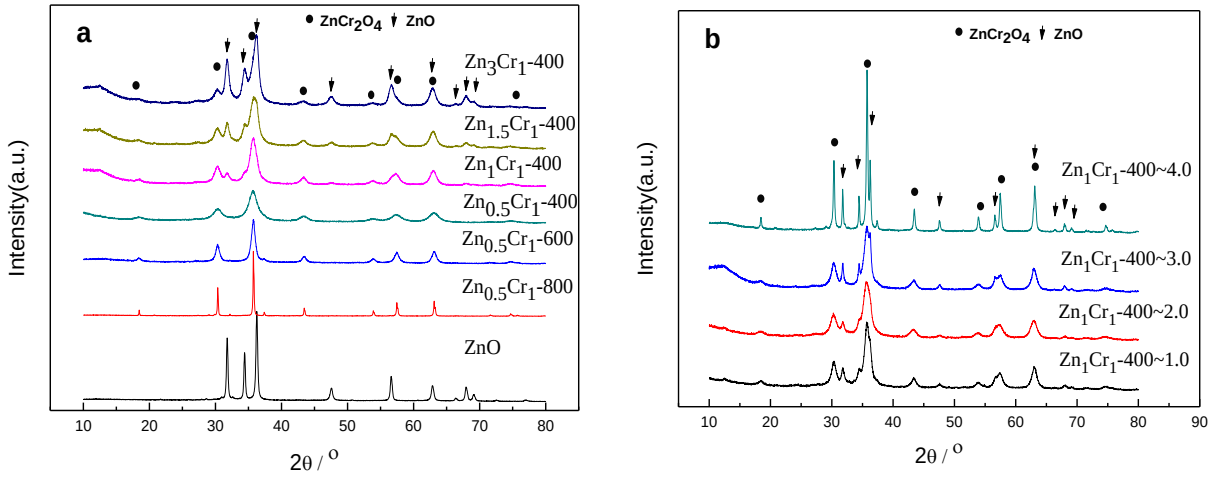

Fig. 1 XRD patterns of the ZnO, Zn_xCr_1-y and Zn_1Cr_1-400~z catalysts

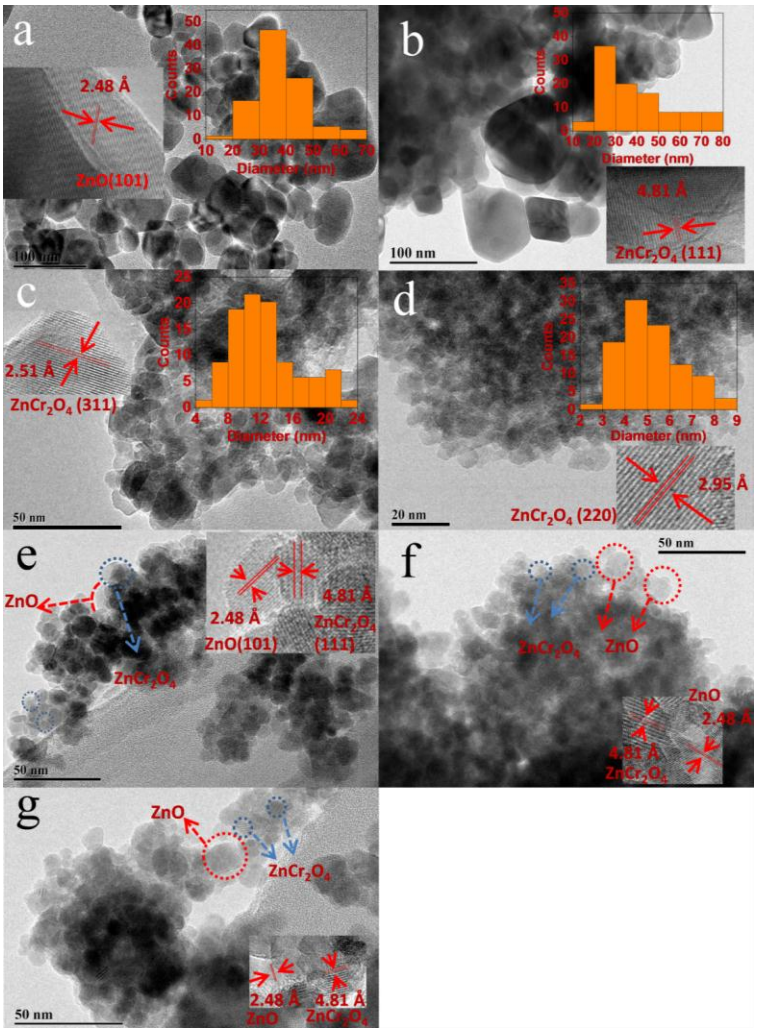

Fig. 2 HRTEM images of different catalysts: (a) ZnO, (b) $Zn_{0.5}Cr_1$-800, (c) $Zn_{0.5}Cr_1$-600, (d) $Zn_{0.5}Cr_1$-400, (e) Zn_1Cr_1-400, (f) $Zn_{1.5}Cr_1$-400 and (g) Zn_3Cr_1-400

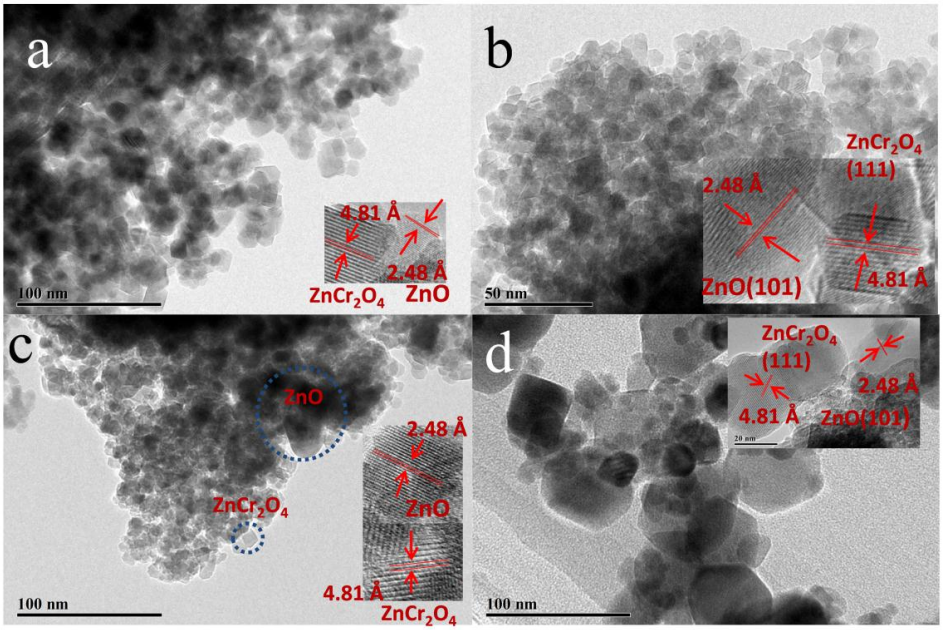

Fig. 3 HRTEM images of different catalysts: (a) Zn_1Cr_1-400~1.0, (b) Zn_1Cr_1-400~2.0, (c) Zn_1Cr_1-400~3.0 and (d) Zn_1Cr_1-400~4.0

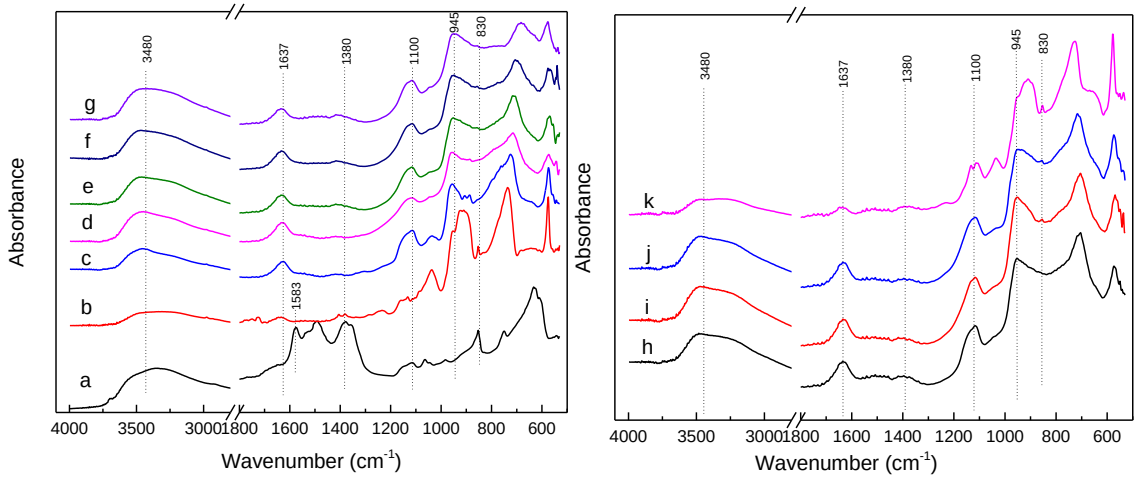

Fig. 4 FT-IR spectrum of different catalysts: (a) ZnO, (b) $Zn_{0.5}Cr_1$-800, (c) $Zn_{0.5}Cr_1$-600, (d) $Zn_{0.5}Cr_1$-400, (e) Zn_1Cr_1-400, (f) $Zn_{1.5}Cr_1$-400, (g) Zn_3Cr_1-400, (h) Zn_1Cr_1-400~1.0, (i) Zn_1Cr_1-400~2.0, (j) Zn_1Cr_1-400~3.0 and (k) Zn_1Cr_1-400~4.0

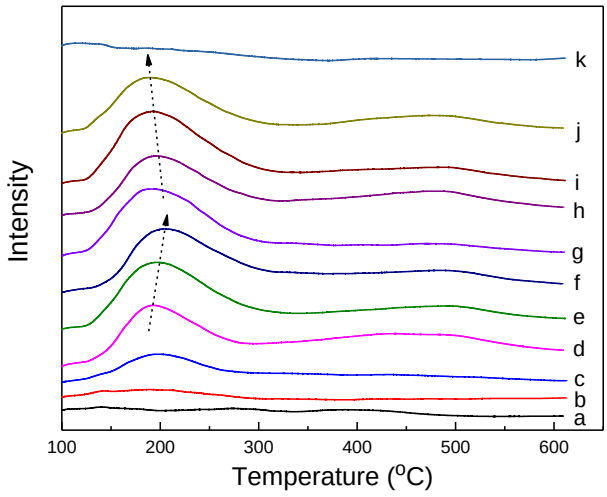

Fig. 5 NH_3-TPD spectrum of different catalysts: (a) ZnO, (b) $Zn_{0.5}Cr_1$-800, (c) $Zn_{0.5}Cr_1$-600, (d) $Zn_{0.5}Cr_1$-400, (e) Zn_1Cr_1-400, (f) $Zn_{1.5}Cr_1$-400, (g) Zn_3Cr_1-400, (h) Zn_1Cr_1-400~1.0, (i) Zn_1Cr_1-400~2.0, (j) Zn_1Cr_1-400~3.0 and (k) Zn_1Cr_1-400~4.0

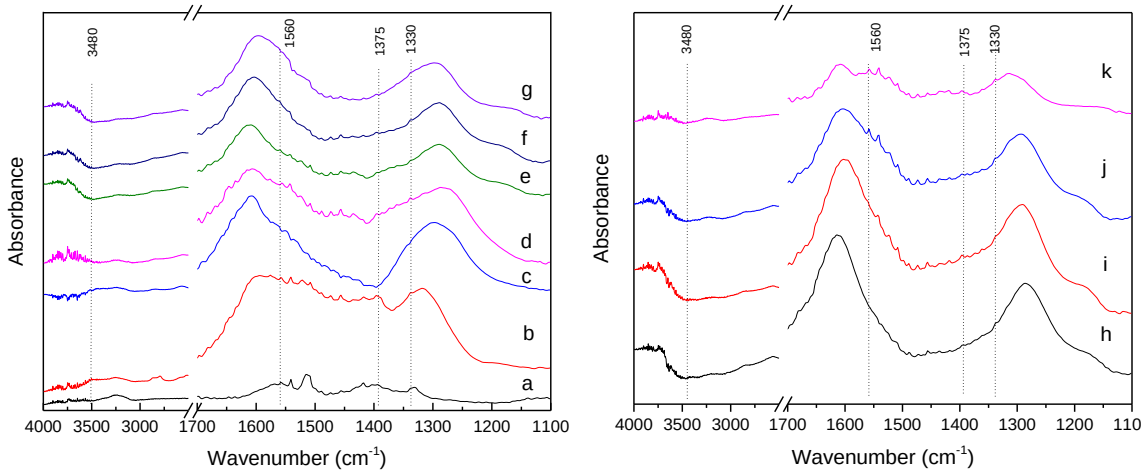

Fig. 6 In-situ CO IR spectrum of different catalysts: (a) ZnO, (b) $Zn_{0.5}Cr_1$-800, (c) $Zn_{0.5}Cr_1$-600, (d) $Zn_{0.5}Cr_1$-400, (e) Zn_1Cr_1-400, (f) $Zn_{1.5}Cr_1$-400, (g) Zn_3Cr_1-400, (h) Zn_1Cr_1-400~1.0, (i) Zn_1Cr_1-400~2.0, (j) Zn_1Cr_1-400~3.0 and (k) Zn_1Cr_1-400~4.0

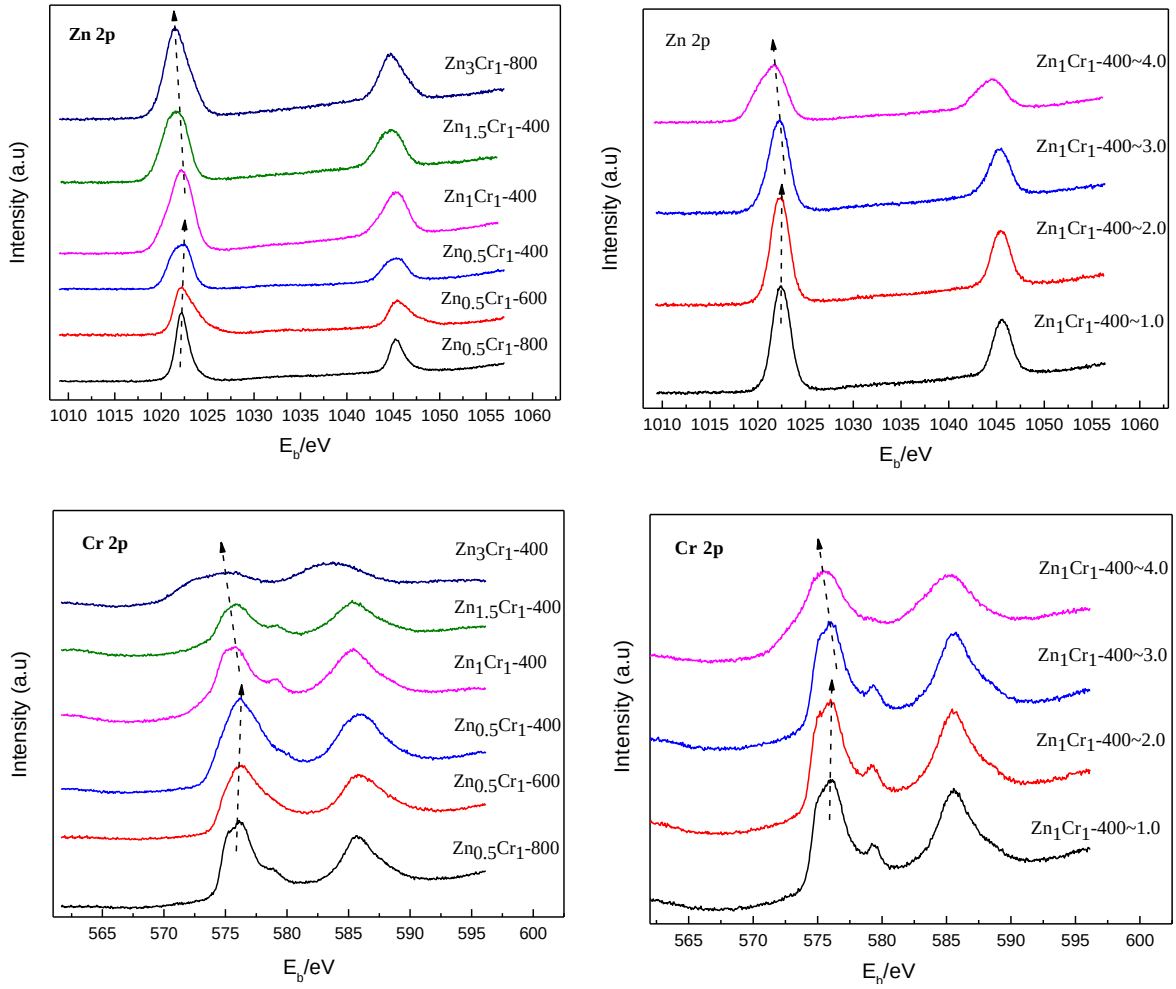

Fig. 7 Zn 2p and Cr 2p XPS spectrum of Zn_xCr_1-y and Zn_xCr_1-y~z catalysts

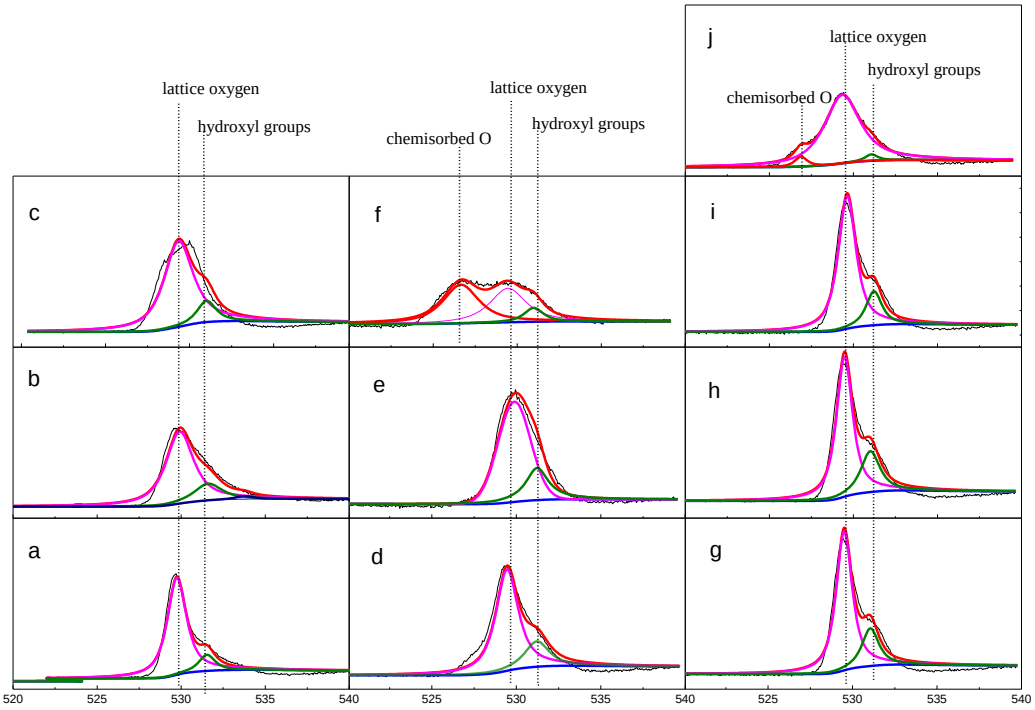

Fig. 8 O 1s XPS spectrum of different catalysts: (a) $Zn_{0.5}Cr_1$-800, (b) $Zn_{0.5}Cr_1$-600, (c) $Zn_{0.5}Cr_1$-400, (d) Zn_1Cr_1-400, (e) $Zn_{1.5}Cr_1$-400, (f) Zn_3Cr_1-400, (g) Zn_1Cr_1-400~1.0, (h) Zn_1Cr_1-400~2.0, (i) Zn_1Cr_1-400~3.0 and (j) Zn_1Cr_1-400~4.0

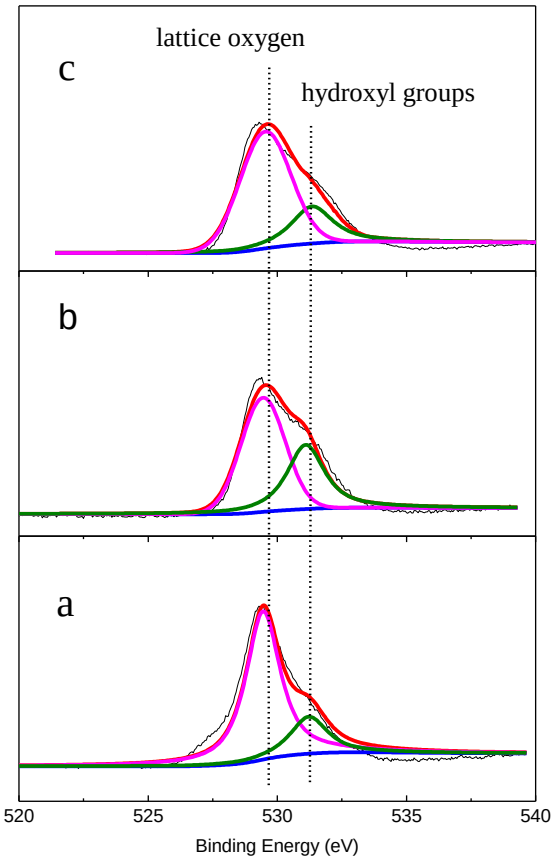

Fig. 9 The XPS spectrum of different catalysts: (a) Zn_1Cr_1-400, (b) in-situ H_2 reduction of Zn_1Cr_1-400, (c) in-situ CO of Zn_1Cr_1-400 performed after H_2 pretreatment at 400 °C for 2h

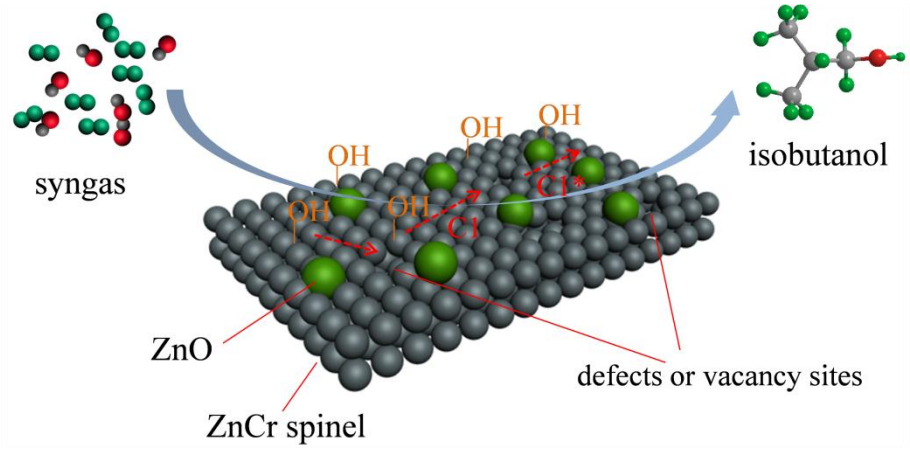

Fig. 10 Schematic diagram of isobutanol synthesis from syngas over ZnCr catalyst

Table 1 The catalytic performance of different catalysts for isobutanol direct synthesis from syngas

Catalysts	CO Conversion (%)	Alcohol Selectivity (%)	Total alcohol production rate ($g \cdot mL^{-1} \cdot h^{-1}$)	C-Balance (%)	Alcohol distribution (wt%)				
					MeOH	EtOH	n-PrOH	i-BuOH	$C^{5+}OH$
ZnO	16.8	21.6	0.050	101.5	78.7	7.4	7.3	2.9	0.4
$Zn_{0.5}Cr_1$-800	10.6	11.4	0.014	100.4	77.6	13.1	6.3	1.6	0.9
$Zn_{0.5}Cr_1$-600	11.1	24.6	0.037	102.1	82.7	4.7	3.9	7.3	1.1
$Zn_{0.5}Cr_1$-400	11.3	60.1	0.051	100.5	81.0	1.3	0.9	14.7	0.5
Zn_1Cr_1-400	16.8	67.3	0.098	99.2	69.6	3.1	3.9	20.9	1.6
$Zn_{1.5}Cr_1$-400	16.2	60.7	0.092	100.1	68.7	3.6	4.6	20.6	1.5
Zn_3Cr_1-400	13.1	51.7	0.066	99.4	76.8	4.3	5.0	11.8	1.2
Zn_1Cr_1-400~1.0	19.3	52.0	0.101	102.1	63.9	3.6	5.1	23.7	2.0
Zn_1Cr_1-400~2.0	20.9	55.8	0.103	100.8	64.6	3.1	4.3	24.2	2.4
Zn_1Cr_1-400~3.0	19.8	52.8	0.102	98.2	64.8	3.5	4.6	19.9	1.8
Zn_1Cr_1-400~4.0	13.0	45.5	0.045	101.2	79.0	7.1	7.0	4.6	0.6

Reaction conditions: temperature = 400 °C, pressure = 10.0 Mpa, GHSV = 3000 h^{-1}.

Table 2 The O species composition of different catalysts

Catalysts	$O_{OH^-}/(O_{latt} + O_{OH^-})$
$Zn_{0.5}Cr_1$-800	12.37%
$Zn_{0.5}Cr_1$-600	18.90%
$Zn_{0.5}Cr_1$-400	19.14%
Zn_1Cr_1-400	21.11%
$Zn_{1.5}Cr_1$-400	24.91%

Zn_3Cr_1-400	17.92%
Zn_1Cr_1-400~1.0	22.11%
Zn_1Cr_1-400~2.0	25.52%
Zn_1Cr_1-400~3.0	18.39%
Zn_1Cr_1-400~4.0	3.192%
In-situ H_2 of Zn_1Cr_1-400	39.65%
In-situ CO of Zn_1Cr_1-400	26.32%

Table 3 Surface compositions of Zn_1Cr_1-400 by XPS analysis under different treatment conditions

Catalysts	Zn (atom ratio%)	Cr (atom ratio%)	O (atom ratio%)	K (atom ratio%)
Zn_1Cr_1-400	21.07	24.28	52.28	2.45
in-situ H_2 of Zn_1Cr_1-400	21.29	24.11	51.97	2.62
in-situ CO of Zn_1Cr_1-400	20.81	26.04	48.14	2.80